Q. J. R. Meteorol. Soc. (2003), **129**, pp. 2591–2611 doi: 10.1256/qj.02.17

Model study of the North Atlantic region atmospheric response to autumn tropical Atlantic sea-surface-temperature anomalies

By MARIE DRÉVILLON[1]*, CHRISTOPHE CASSOU[2] and LAURENT TERRAY[1]

[1] *CERFACS/CNRS, URA1875-SUC, Toulouse, France*
[2] *NCAR, Boulder, USA*

(Received 24 January 2002; revised 17 March 2003)

SUMMARY

Lead–lag Maximum Covariance Analysis (MCA) between National Centers for Environmental Prediction reanalysis sea surface temperature (SST) and 500 hPa geopotential-height fields shows that autumn tropical Atlantic SST anomalies are significantly linked with the following-winter North Atlantic Oscillation (NAO). The ability of the Météo-France atmospheric general circulation model ARPEGE to reproduce this relationship is tested, by forcing it with autumn tropical SST anomalies derived from lead–lag MCA analysis results. The autumn SST forcing induces a strong wave-like simultaneous response in October and November. The occurrence of the autumn weather regimes is also affected, in agreement with the significant spatial correlation of the midlatitude part of the wave response with the NAO pattern. By coupling the model with a slab ocean in midlatitudes, we show that the thermal coupling between the ocean and the atmosphere allows a better representation of the midlatitude part of the response. A negative autumn tropical SST anomaly triggers an interaction between the midlatitude SST, the low-frequency circulation and the storm-track activity, which reinforces and maintains a positive phase of the NAO until winter.

KEYWORDS: Mixed layer NAO Ocean–atmosphere interaction Storm track Wave–wave interactions

1. INTRODUCTION

In order to investigate the origins of winter climate variability in the North Atlantic Europe (hereafter NAE) region and to further improve climate prediction, many studies have focused on the influence of either midlatitude or tropical Atlantic sea surface temperature (SST) on low-frequency atmospheric variability. Since the study of Bjerknes (1964), it is generally admitted that the principal midlatitude SST mode, called the 'tripole', varies synchronously with the North Atlantic Oscillation (NAO). The former comprises latitudinal band anomalies of the same polarity in the subtropics and south of Greenland, and a central anomaly of opposite polarity. The latter is the principal atmospheric variability mode and is defined by a surface pressure see-saw between Iceland and the Azores. Cayan (1992) shows that the NAO drives the SST tripole through surface heat-flux exchanges. The question of the winter feedback of these SST anomalies on the atmosphere is controversial as it is much smaller than the strong atmospheric forcing of the ocean surface, and thus cannot be distinguished (Frankignoul 1985). Recently Czaja and Frankignoul (1999) identified a relationship between a horseshoe-shaped summer SST anomaly in the North Atlantic ocean (central anomaly at 40°N circled to the east with the opposite polarity anomaly) and the next winter NAO using Maximal Covariance Analysis (MCA), which gives spatial structures in each field that covary in time. This lagged relationship induces predictability in the NAE region on the seasonal scale (Rodwell and Folland 2002). Mechanisms that can be responsible for this relationship are suggested in Drévillon *et al.* (2001), where it is argued that the initial anticyclonic anomaly response to the horseshoe is maintained and amplified by the storm-track activity, resulting in an atmospheric mode that closely resembles the NAO pattern.

* Corresponding author: Climate Modelling and Global Change Project, CERFACS/CNRS, URA1875-SUC, 42, Avenue G. Coriolis, 31057 Toulouse Cédex, France. e-mail: drevillo@cerfacs.fr

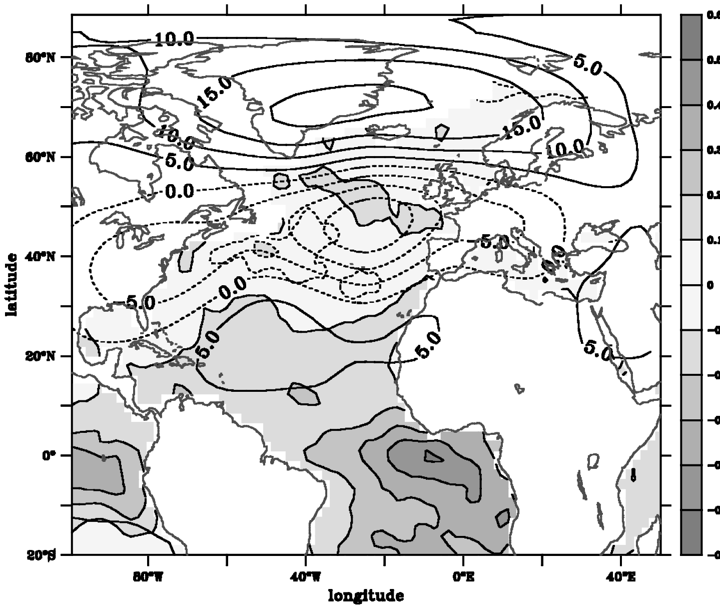

Figure 1. Lagged Maximal Covariance Analysis (MCA) heterogeneous patterns of mean September, October and November (SON) sea surface temperature (SST) (grey levels, thin contours every 0.1 degC) and mean November, December and January (NDJ) 500 hPa geopotential height (thick contours every 5 m), negative values are dashed for both fields. The square covariance fraction of the structures is 68.9%, (significant at the 92% level with respect to a Monte Carlo test) and the correlation coefficient between the MCA time series is 0.53 (significant at 88%).

Part of the atmospheric NAE variability can also be linked to tropical and South Atlantic SST. As in Czaja and Frankignoul (2002), we perform here a lead–lag MCA between the National Centers for Environmental Prediction (NCEP) tropical (20°S to 20°N) Atlantic SST and the Atlantic (20°S to 70°N) 500 hPa geopotential height (hereafter Z500) and find a significant covariance between an east equatorial SST variability pattern in autumn and the next winter NAO (Fig. 1). Czaja and Frankignoul (2002) show that the action of this tropical pattern on the low-frequency atmospheric variability in the North Atlantic region is significant, although weaker than that of the horseshoe pattern. Anomalous SSTs in the eastern tropical Pacific induce north-eastward-propagating atmospheric Rossby waves that can alter the extratropical atmospheric circulation (see Trenberth *et al.* 1998). The same type of mechanism could play a role in the observed tropical Atlantic SST impact on the North Atlantic region atmosphere. As proposed by Sardeshmukh and Hoskins (1988) SST anomalies in the tropics can result in anomalous low-level convergence leading to a modification of convection and thus of the local Hadley circulation. Rossby waves can then be induced by vorticity convergence in the subsiding branch of the Hadley cell. In his review of the interaction between global SST anomalies and the midlatitude atmospheric circulation, Lau (1997) emphasizes the critical importance of air–sea coupling in midlatitudes in amplifying the extratropical response to tropical SST anomalies. Hoerling and Ting (1994) demonstrate the importance of the organization of transient eddies in maintaining the North Pacific midlatitude atmospheric response to El Niño events, which has the spatial structure of the Pacific North American (PNA) teleconnection pattern. Watanabe and Kimoto (1999) prescribe a December, January and February (DJF) tropical Atlantic anomaly (resembling the autumn SST anomaly which covaries with the NAO in the observations) to an atmospheric general-circulation model (AGCM) coupled with a mixed-layer model in the midlatitudes. They show that the response looks closely like the NAO pattern and demonstrate with a baroclinic linear model that the transient-eddy processes are important in stabilizing the response. The equatorial SST anomaly in the eastern part of the Atlantic basin corresponds to the spatial pattern of the second empirical orthogonal function (EOF) of SST variability in the tropical Atlantic, and is not correlated in time with El Niño or the horseshoe pattern. Zebiak (1993) suggested that it is part of an 'Atlantic El Niño' phenomenon, as a reduction of the Atlantic easterly trade winds is observed when the anomaly is positive, as can be seen in the Pacific during El Niño events. Sutton *et al.* (2000), using the optimal filtering technique in an ensemble of forced simulations, found that fluctuations of SST in the tropical Atlantic are likely to influence the tropical atmospheric variability, especially during the mean season September, October and November (SON).

The aim of the present study is to assess with various sensitivity experiments the capability of an AGCM to reproduce the observed statistical lagged relationship between the autumn tropical SST anomaly and the next winter NAO. The numerical experiments then allow us to better investigate the physical processes that can induce this link, and especially the role played by the transient eddies in the midlatitudes. The observed autumn tropical SST structure, varying in time from September to November, is prescribed in the AGCM either coupled or not coupled with a slab ocean model in the midlatitudes. Ensembles of simulations are made that allow us to study the atmospheric response to this SST anomaly, the impact of thermal coupling at the atmosphere–ocean interface on the spatial structure and the persistence of the atmospheric response is discussed.

In section 2 the two different model designs are described, and briefly validated. The physical diagnostics as well as the statistical analyses to be performed on the sensitivity experiments are detailed. The autumn atmospheric response for each set of ensemble experiments is described in section 3. Mechanisms that could be responsible for the low-frequency response to tropical SST forcing, and the modulation of this response at midlatitudes are examined. The winter atmospheric response is described in section 4. The principal conclusions of this study are given in section 5.

2. Model experiments and analysis tools

(*a*) *Model presentation*

The ARPEGE Integrated Forecasting System (IFS) AGCM, jointly developed by Météo-France and the European Centre for Medium-Range Weather Forecasts (ECMWF), is described in Dequé *et al.* (1994). ARPEGE is a spectral model with truncation T63 for the description of the dynamics. The model was run here with 31 levels in the vertical, the physical and dynamical fields are displayed on a 2.8 degree × 2.8 degree horizontal grid. This configuration of the model resolves the synoptic-scale transient eddies, and correctly simulates the NAE region winter climate variability on the intraseasonal (Doblas-Reyes *et al.* 1998, 2001) and interannual (Cassou and Terray 2001) time-scale. The first control simulation (hereafter called C) is done by integrating ARPEGE for 30 years with prescribed climatological NCEP SST.

The same version of ARPEGE can be coupled with a slab-ocean mixed-layer model in the North Atlantic basin (here between 25°N and 60°N with 10° buffer zones in latitude). This allows the thermal coupling to take place in the model between the ocean and the atmosphere in the North Atlantic region. The oceanic mixed-layer model has a seasonally varying depth, which can play an important role in the representation of climate variability by the model and a flux correction is applied to avoid the temperature drift. This flux correction can be considered to be a compensation for the absence of advection of heat in the mixed-layer model. A 30-year control simulation (hereafter C_{ML}) is thus performed with this second model configuration, with the oceanic mixed layer in the midlatitudes and climatological SSTs everywhere else.

These two control simulations will serve as references to study the impact of prescribing different SST anomalies in both configurations of the model.

(*b*) *Preliminary validation of the control simulations*

If the atmospheric internal-variability spatial structures are not correctly reproduced by the model, its response to prescribed SST anomalies can be distorted (Peng and Robinson 2001). In order to make a short validation of the two model configurations, we describe here the first EOF of autumn, October and November (ON), and winter, January and February (JF), mean 500 hPa geopotential height (hereafter referred to as Z500) in C and C_{ML}, and in the NCEP re-analysis dataset. The observed autumn NAO (Fig. 2(a)) has a wave-like spatial structure, arching north-eastward and ending with an anticyclonic anomaly over Scandinavia. The first autumn EOF of C (Fig. 2(b)) depicts a zonal atmospheric circulation over the Atlantic and western Europe. The first autumn mode of C_{ML} (Fig. 2(c)) displays spatial structures of variability that more closely resemble those observed. The superimposed Plumb vectors in Figs. 2(a), (b) and (c), are obtained by regressing the mean ON Plumb vectors on the temporal coefficients of the EOF (40 years for the NCEP dataset and 30 for C and C_{ML}). They show stationary wave-activity fluxes associated with the mode, which happen to be better represented in C_{ML} than in C with respect to the NCEP re-analysis, especially in the eastern part of the basin. In Fig. 2(a) a flux anomaly is directing wave-activity energy south-west from the British Isles, this can also be found, shifted westward, in Fig. 2(c). The Icelandic low is underestimated for both C and C_{ML} JF NAO dipoles (Figs. 2(e) and (f)) and shifted to the north-west with respect to the observed one (Fig. 2(d)), and the amplitude of the Azores high is overestimated in the control experiments. This results in a north-westward shift of the maximum horizontal pressure gradient. The associated wave energy flux is more zonally oriented than in the observations. The east Atlantic ridge (second mode, not shown), consisting of a strong anticyclonic anomaly in the centre of the North Atlantic basin, is underestimated in amplitude. These misrepresentations may be due to the zonality of the northern-hemisphere westerly flow in ARPEGE, introducing biases in the climatological stationary waves (Doblas-Reyes *et al.* 1998) and a too strong Pacific–Atlantic connection implying Pacific North American (PNA) teleconnection extension over Europe (Cassou and Terray 2001). The reader is invited to refer to these two articles for a comprehensive validation of ARPEGE. The biases described here, which are shared by other AGCMs like the National Center for Atmospheric Research (NCAR) Community Climate Model Version 3 (CCM3) (Hurrell *et al.* 1998), will be taken into account when discussing the model's response to SST anomalies.

(*c*) *Sensitivity experiments*

The sensitivity of ARPEGE to the autumn tropical SST anomaly is assessed by performing ensembles of atmospheric simulations, forced with monthly varying SST anomalies. The length of these integrations is 9 months (from July to March). The prescribed anomalous SST patterns are derived as follows. For the autumn forcing patterns,

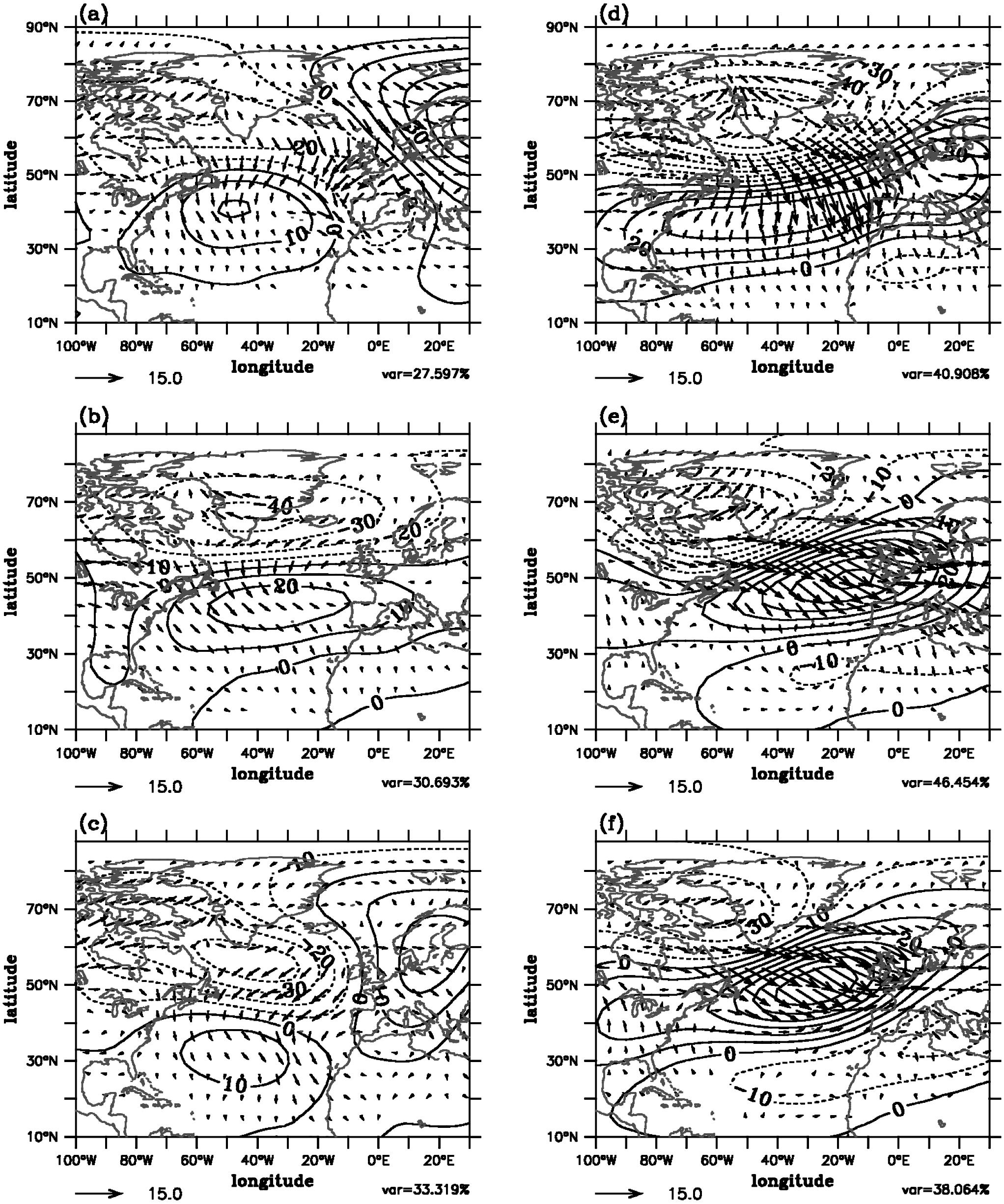

Figure 2. First empirical-orthogonal-function spatial patterns of mean October and November (ON) 500 hPa geopotential height (Z500) and mean January and February (JF) Z500, (a) and (d) for the National Centers for Environmental Prediction/National Center for Atmospheric Research re-analysis dataset, (b) and (e) for C, and (c) and (f) for C_{ML} (see text). The contour interval is 10 m. Plumb vectors $\mathbf{F}$ ($m^2 s^{-2}$) regressed on the corresponding time series are superimposed. The percentage of variance explained by the structures is indicated for each one of them in the lower right corner.

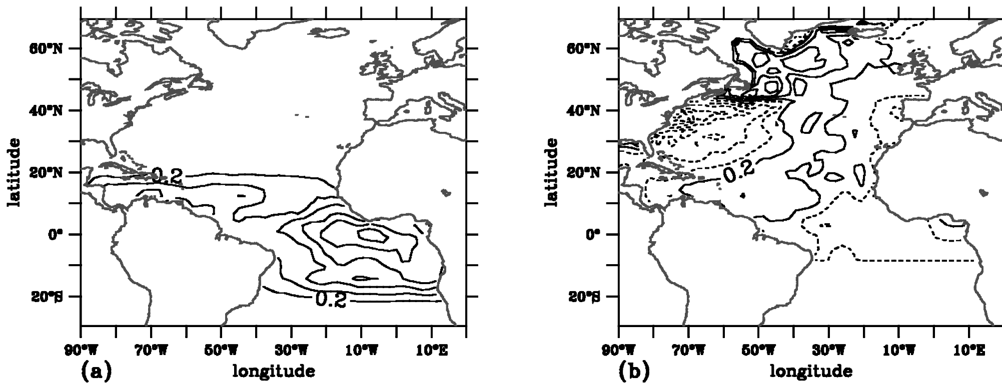

Figure 3. Sea-surface-temperature forcing pattern of (a) September, and (b) December, contours every 0.2 degC.

NCEP monthly SST maps of September, October and November are separately regressed upon the time series (not shown) of the MCA SST pattern of Fig. 1. The September 20°S–20°N SST forcing pattern obtained is displayed in Fig. 3(a), the October and November maps are not shown as the main features of the anomaly are persistent.

For the winter forcing patterns, NCEP monthly SST maps of December, January and February are regressed upon the time series of the North Atlantic (from 0°N to 70°N) tripole obtained by a synchronous MCA between Z500 and SST in the North Atlantic domain. The tripolar forcing structure is displayed here for December (Fig. 3(b)), the main features of the January and February patterns being similar. The sign of the tripole is chosen here as if this midlatitude SST anomaly was resulting from surface heat-flux exchanges between the atmospheric response to the preceding autumn tropical SST anomaly, and the North Atlantic oceanic mixed layer. Therefore, in the case of a positive (negative) tropical SST anomaly in autumn, the following tripole consists of a positive (negative) basin-wide subtropical SST anomaly in the 0–20°N latitude band, a negative (positive) anomaly between 20°N and 40°N and a positive (negative) anomaly to the north, from the Labrador Sea and Newfoundland to the Irish coasts.

For the remaining months, no SST anomalies are prescribed. The daily SST values used to force the ARPEGE model are obtained through linear interpolation in order to smooth the transition between the monthly mean SST anomalies. Those SST patterns are used to force ensembles of 15 simulations (called members), which are made independent by varying their initial atmospheric conditions (different days at the beginning of July, taken from the C simulation). The atmospheric response to the forcing is obtained by averaging the members, which filters out most of the atmospheric chaotic behaviour.

We performed four different ensembles of atmospheric simulations. The tropical (from September, Fig. 3(a) to November) and then midlatitude (from December, Fig. 3(b), to February) SST time-varying forcing is added to the NCEP climatological SST for the first ensemble. Another ensemble of the same length is performed for the opposite polarity of the forcing, in order to estimate the linearity of the response. For convenience, these ensemble experiments will hereafter be referred to as, respectively, P (positive equatorial anomaly followed by positive/negative/positive tripole) and N (negative equatorial anomaly followed by negative/positive/negative tripole).

A second set of 15-member ensembles of 9 months (from July to March) is obtained by integrating ARPEGE coupled with the mixed-layer model in the North Atlantic and forced by NCEP climatological SSTs everywhere else, as described in section 2(a). In September, October, and November the tropical SST anomalies (September forcing displayed in Fig. 3(a)) are added to the climatological SST. No SST anomaly is prescribed in the North Atlantic basin in winter as the coupling with the slab ocean takes place in this region. A positive ensemble of coupled sensitivity experiments (hereafter P_{ML}) and a negative one (N_{ML}, forcing of opposite sign) are then performed.

(*d*) *Defining and analysing the response*

(i) *Linear and nonlinear response.* The linear part of the sensitivity experiments' response to the SST forcing can be estimated in a simple way. $\langle L \rangle = (\langle P \rangle - \langle N \rangle)/2$ gives the part of the response which is symmetric with respect to the sign of the forcing. The brackets which here denote the ensemble mean will be omitted in the following sections. The mixed-layer coupled sensitivity-experiment linear response will also be estimated by $\langle L_{ML} \rangle = (\langle P_{ML} \rangle - \langle N_{ML} \rangle)/2$. The nonlinear part of the response can be estimated by computing the departures from the corresponding control simulations, as $\langle P \rangle - \langle C \rangle$ or $\langle P_{ML} \rangle - \langle C_{ML} \rangle$.

(ii) *Frequency–wave-number spectral analysis.* Following the method of Doblas-Reyes *et al.* (2001), a frequency–wave-number spectral analysis or space–time spectral analysis, developed by Hayachi (1971), is applied to our experiment's Z500 field. In addition to classical spectral analysis, this method allows us to assess the contributions of travelling and standing waves to the total space–time transient variance of the Z500 field. The Z500 field is first separated into longitude (90°W–90°E) versus time (in days, depending on the season studied) series for each latitude of the atmospheric grid from 20°N to 80°N. The zonal and time mean are substracted and, by means of a Fourier transform along the longitudes, the remaining space–time transient series are expanded into zonal Fourier coefficients, thus varying with latitude and time. For each latitude, the space-time spectra and cross-spectra are obtained by a classical spectral analysis of the Fourier coefficients. These are then used following the method of Pratt (1976) to separate the standing-wave and the propagating-wave variances. A thorough description of the method and its limitations is given in Von Storch and Zwiers (1999), and a detailed comparison of ARPEGE results with the observations is made by Doblas-Reyes *et al.* (2001).

(ii) *Cluster analysis.* One way to consider the nonlinear and high-frequency response to the various types of forcings of our sensitivity experiments is to adopt the weather-regimes approach. Weather regimes are usually defined as peaks in the probability density function (PDF) of the phase space of climate. The hypothesis can be made that a modification of the climate mean state or variability due to an external forcing will result in a change in the amplitude of these peaks, or in the preferred transitions between them (Corti *et al.* 1999). Under this hypothesis, one should observe more or less occurrences of pre-existing weather regimes in response to an SST forcing, rather than the appearance of new ones. Thus, the response of the model can be studied by comparing the frequencies of occurrence of the principal weather regimes between the various sensitivity experiments. Daily maps of sea level pressure (SLP) of the various sensitivity experiments are classified into weather regimes following the k-means method described in Michelangeli *et al.* (1995). Classification is performed on the first ten principal components of the anomalous daily SLP maps, by minimizing the quadratic distance to a specific number of arbitrarily predetermined centroids. For this specific number, the classification is performed a hundred times with a different set of arbitrarily determined centroids, in order to test the robustness of the cluster partition. The partition retained is the one that correlates best with the 99 others. A classificability index is based on the latter correlation coefficient computed for different numbers of centroids, the optimal number of centroids (or clusters, or regimes) being given by its highest value.

Either a change in the mean response or a change in variability can be interpreted in terms of a modification of frequency of occurrence of the intrinsic weather regimes of the model. In order to estimate the change in the mean response that can be accounted for by the regime occurrence changes, we follow here the method described in Farrara *et al.* (2000). For each set of three ensembles (forced P, N, and C, or coupled with slab ocean P_{ML}, N_{ML} and C_{ML}) anomalous daily maps of SLP with respect to the corresponding control ensemble mean are classified together with the k-means algorithm. Note that the classifications of the two kinds of ensembles give the same regimes (which are spatially correlated at more than 0.9). The differences in the frequency of occurrence of a specific regime between the ensembles of one kind are considered significant if they largely exceed the sampling error margin given by the 'within-ensemble variability'. The latter is obtained by substracting the mean of the relevant ensemble from the original SLP daily maps. Then for each set of three ensembles, these new anomalous SLP maps are classified together with the k-means algorithm. The maximum difference in the frequency of occurrence of a specific weather regime between the positive, negative and control ensemble of one kind then quantifies the 'within-ensemble variability' of the regime.

(*e*) *Diagnostic of the physical processes of the response*

The Rossby Wave Source (RWS) derived from the vorticity equation is defined by Sardeshmukh and Hoskins (1988) as

$$\mathrm{RWS} = -\overline{\mathbf{v}_\chi \cdot \nabla(\zeta + f)} - \overline{(\zeta + f)D}, \tag{1}$$

where $\mathbf{v}_\chi$ is the divergent part of the 200 hPa wind, ζ is the relative vorticity, f the Coriolis parameter and D the divergence at 200 hPa. The RWS quantifies the vorticity source induced by low-level convergence and upper-level divergence associated with an anomalous heating in the tropics.

The Plumb vector **F**, defined in Plumb (1985), is a diagnostic tool for the three-dimensional stationary-wave activity. It is derived from a locally applicable conservation relation for quasi-geostrophic waves on a zonal flow, and here computed as in Fraedrich *et al.* (1993). An anomalous divergence (convergence) of the **F** vectors depicts a region of creation (dissipation) of an anomalous quasi-stationary wave. **F** is also perpendicular to the wave front of stationary waves.

The synoptic-scale transient-eddy activity, hereafter referred to as Storm-Track Activity (STA), is defined following Hoskins and Valdes (1990) by $\sqrt{\overline{z'^2}}$, where z is the 500 hPa geopotential height, and the prime refers to band-pass (2.2–6 days) filtered daily data. The Eliassen–Palm vector **E** gives a description of the transient-eddy forcing upon the local time-mean flow. Following Trenberth (1986) its zonal and meridional components are defined, respectively, by the momentum flux of the transient eddies $-\overline{u'v'}$, and $1/2(\overline{v'^2} - \overline{u'^2})$, where u and v are the band-pass filtered zonal and meridional components of the wind at 200 hPa. The divergence of **E** depicts the eddy-induced accelerations of the zonal wind due to barotropic processes. In the barotropic case,

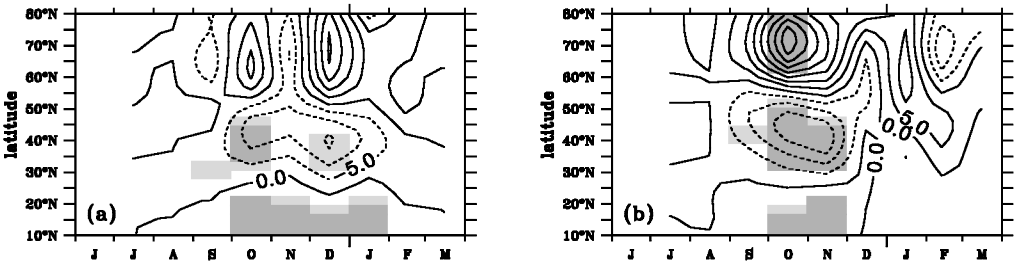

Figure 4. Latitude–time diagram of the 500 hPa geopotential height (Z500) linear response, (a) L and (b) L_{ML} (see text) averaged over the 100°W–30°W longitude band. Contour interval 5 m. Statistical significance of the response is assessed with a two-tailed t-test with O(60) degrees of freedom, as the variance is estimated with all the experiments of one type (forced or coupled). Significant regions over the 95% level are shaded in dark grey, and over 90% in light grey.

E is in the direction of the group velocity of the transient eddies relative to the local time-mean flow.

Low-level baroclinicity (here at 700 hPa) is quantified by the Eady baroclinic-instability growth-rate maximum

$$\sigma_{\mathrm{BI}} = 0.31 f \left| \frac{\partial \mathbf{u}}{\partial z} \right| N^{-1}, \tag{2}$$

where **u** is the zonal wind, and N is the Brunt–Väisälä or buoyancy frequency, as in Hoskins and Valdes (1990).

3. Modelled atmospheric response to the autumn SST anomaly in the tropical Atlantic

The 30°W–100°W averaged latitude–time diagram of the Z500 linear response is displayed in Fig. 4. For both types of sensitivity experiments, a statistically significant large-scale response takes place in October and November. It is worth noting that the L_{ML} response is stronger and more persistent at high latitudes, whereas the L response seems to disappear in November and reappear later in December and January, and stays significant in the subtropics from October to January. In the present section, we study the mean ON atmospheric response, and in section 4 the JF atmospheric response. We choose these two specific two-month averages in order to study separately the respective influences of the tropical SST structure and of the midlatitude SST tripole.

(*a*) *A wave-like October and November atmospheric response*

The mean ON Z500-response spatial structure (Fig. 5) exhibits a wave-like structure that resembles the model NAO dipole in ON, in both L and L_{ML} (respectively, Figs. 2(b) and (c)). This structure conforms to what we would expect from the observed linear relationship of Fig. 1, with a zonal average negative anomaly at 45°N and a positive one at 70°N. The stronger amplitude of the L_{ML} response is notable here, especially in the mid and high latitudes, west of 20°W. Moreover, the L_{ML} response over Europe bears the opposite sign to that in the western part of the Atlantic basin, which matches the Fig. 2(c) north-eastward-tilted autumn NAO. Nevertheless, the significant part of the L_{ML} Z500 wave train seems to be confined to the western part of the basin, and a cyclonic anomaly can be observed over north Africa in both L and L_{ML} responses, which is not an NAO signature according to Fig. 2. In both types of simulations the vertical

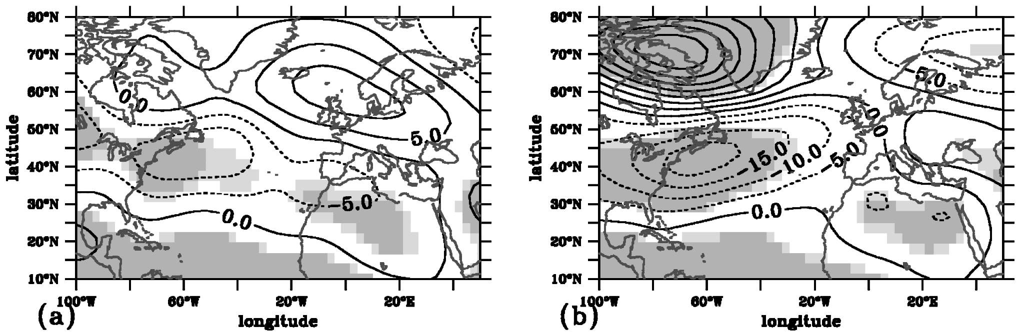

Figure 5. Spatial structure of the 500 hPa geopotential-height linear response in October and November for (a) L and (b) L_{ML} (see text). Contour interval 5 m. Statistical significance shading as in Fig. 4.

structure of the response to a positive SST anomaly consists of a baroclinic ridge in the tropics, a barotropic low at 40°N and a barotropic ridge at 70°N (not shown) consistent with a Rossby wave propagating meridionally from the tropics. We also notice that the L_{ML} response is stronger and significant at all levels in the midlatitudes. In ON, the whole tropical–subtropical-band high-level atmospheric response displays a pair of ridges straddling the equator (not shown). The maximum of the southern-hemisphere ridge is located near 80°W over Peru, and the ridge itself extends over the South Atlantic to the west African coasts. The northern-hemisphere ridge is also a maximum near 80°W, over the Caribbean Sea, and extends more into the African continent. In ON, a local Hadley cell ascending branch is located near 5°S and 80°W.

Hoskins and Ambrizzi (1993) show that the winter DJF response of a barotropic model to a forcing localized at the equator and 90°W (near the ascending branch of the Hadley cell) is a north-eastward wave propagating in this particular direction due to the wave-guide properties of the North Atlantic jet stream. In our case, the wave train is shorter and an anomalous low is found over the Gulf of Alaska. These differences might be due to the different spatial structures of the ON teleconnections, and different properties of the jet stream and Hadley cell in this season. Pacific teleconnections may also be excited in the model by the perturbation of the Walker circulation, overestimated by ARPEGE. We will focus here on the Atlantic region wave.

Consistent with Hoskins and Ambrizzi (1993), an anomalous convergence of heat actually takes place in ON in our experiments, it is located in the Amazon region, at the equator and between 40°W and 80°W, as can be seen in Fig. 6. It is associated with anomalous moisture convergence in the same region (not shown). The low-level (850 hPa) transport of heat is dominated by the transport of mean temperature by the anomalous wind $\langle \mathbf{v}_{L_{ML}} T_{C_{ML}} \rangle$ (Fig. 6(a)) but the transport of anomalous temperature by the mean easterly flow $\langle \mathbf{v}_{C_{ML}} T_{L_{ML}} \rangle$ (Fig. 6(b)) also plays a non-negligible role. The addition of these two terms reinforces the convergence of heat over the Amazon region. This low-level anomalous convergence induces an amplification of convection and of upper-level divergence. The local Hadley cell is thus altered and anomalous advection of vorticity by the divergent wind can initiate a Rossby wave. In order to determine if a Rossby wave is forced in the Caribbean Sea region in our sensitivity experiments, RWS, as defined in section 2(e), is computed for both L and L_{ML}. A dipole of RWS appears in Fig. 7 between 80°W and 100°W corresponding to anticyclonic forcing between 5°N and 20°N and to cyclonic forcing between 20°N and 30°N, consistent with the L and L_{ML} atmospheric response of Fig. 5. The negative anomaly

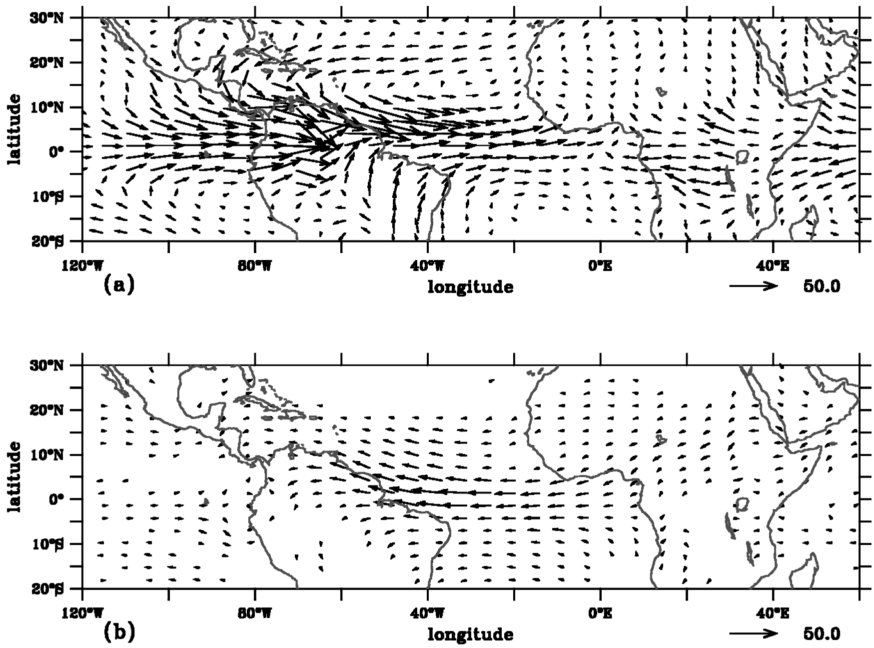

Figure 6. October and November (a) low-level (850 hPa) transport of mean C_{ML} temperature by the anomalous L_{ML} wind $\langle \mathbf{v}_{L_{ML}} T_{C_{ML}} \rangle$ (K m s^{-1}), and (b) low-level transport of anomalous L_{ML} temperature by the mean C_{ML} wind $\langle \mathbf{v}_{C_{ML}} T_{L_{ML}} \rangle$ (K m s^{-1}). See text for further explanation.

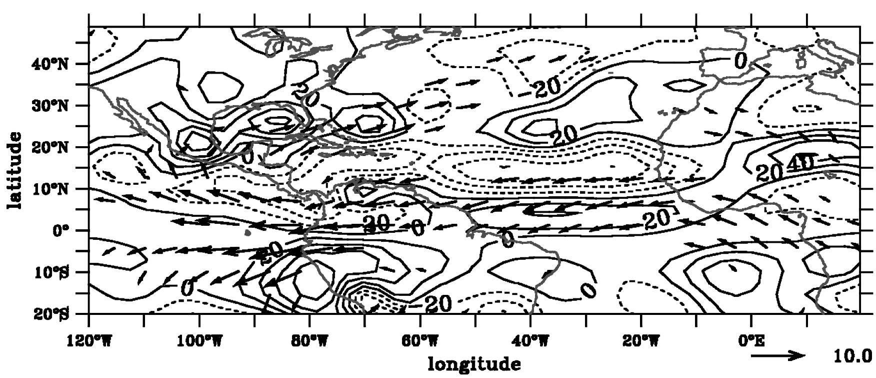

Figure 7. October and November Rossby Wave Source (RWS) at 200 hPa for L_{ML}. Contour interval is 20×10^{-11} s^{-2} and negative values are dashed. Anomalous L_{ML} wind significant at the 90% level is superimposed. See text for further explanation.

above central America corresponds to advection of vorticity by the anomalous divergent wind. The 200 hPa wind anomaly depicts an acceleration driven by the anticyclonic anomaly. The northern part of the RWS dipole is essentially due to anomalous vortex stretching by the divergence $-\overline{(\zeta + f)D}$ from Eq. (1), which is important for the stabilization of the wave response in the midlatitudes as pointed out by Qin and Robinson (1993).

A mechanism can be proposed following Tyrrell *et al.* (1996) which involves the local Hadley cell emanating from the Amazon region, where strong convection takes

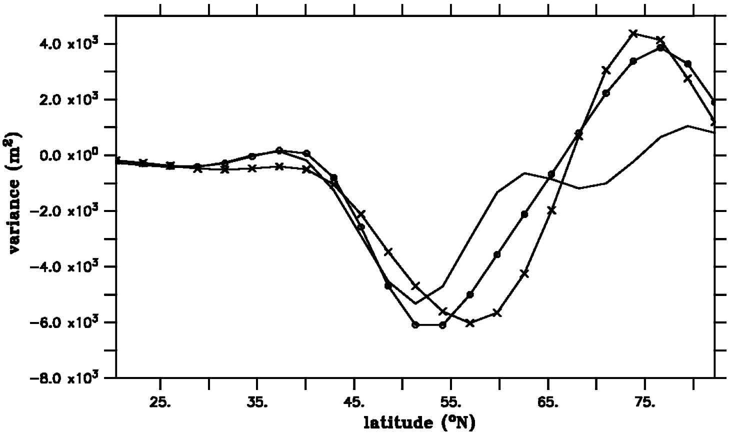

Figure 8. October and November propagating-wave variance (m^2) integrated in the region $k = 1$ and $t = 6.6$ to 61 days of the respective spectrum for P_{ML} (crosses), N_{ML} (circles) and C_{ML} (solid line). Negative sign indicates westward propagation. See text for further explanation.

place. Enhanced convection in the lower-latitude part of the local Hadley cell induces advection of vorticity by the anomalous divergent wind in the higher-latitude subsiding branch of the cell. In this area the Rossby source term is large due to stretching of the absolute vorticity. Then, this large resultant RWS causes the propagation of a Rossby wave from the region of the downward branch of the Hadley cell. The region being the entrance of the North Atlantic jet stream, the upper-level wave can then be driven north-eastward by the jet.

This propagating Rossby wave, or its influence on the midlatitude circulation, may be distinguished in the ON L_{ML} space–time spectrum of the Z500 variance, as defined in section 2(d). The differences between the spectra of the P_{ML} and N_{ML} experiments are essentially due to planetary-scale waves of periods longer than 10 days and of wave numbers k =1–3 (not shown). The variances of planetary-scale propagating waves in P_{ML} and N_{ML} can be computed for all latitudes by integrating the propagating variance spectra in the relevant wave numbers and periods ($k = 1$ and periods from 6.6 to 61 days). The latitude/variance diagram obtained is displayed in Fig. 8. The preliminary observation can be made that C_{ML} variance of the westward-travelling planetary-scale waves between 30°N and 75°N is well simulated with respect to the ECMWF re-analysis shown in Doblas-Reyes *et al.* (2001). Both P_{ML} and N_{ML} display more variance in the high latitudes than C_{ML}, a signature of eastward-propagating waves. In P_{ML} with respect to C_{ML}, the westward-travelling wave's variance is enhanced between 52°N and 65°N, and reduced to the south between 40°N and 52°N, shifting the variance maximum about 10° northward. This shift of the longitudinal waves is consistent with the stronger boreal-winter local Hadley cell in response to the warm tropical SST anomaly. It is also consistent with a westward-propagating wave response to the tropical forcing in ON. The negative equatorial SST anomaly forcing also induces an enhancement of the propagating wave's variance in the extratropics between 47°N and 65°N, in N_{ML} with respect to C_{ML}. The integration of the spectra for $k = 2$ (not shown), shows more propagating- and stationary-wave variance enhancement in P_{ML} than in N_{ML} with respect to C_{ML}, suggesting more propagating-wave activity in general in the warm SST-forcing case.

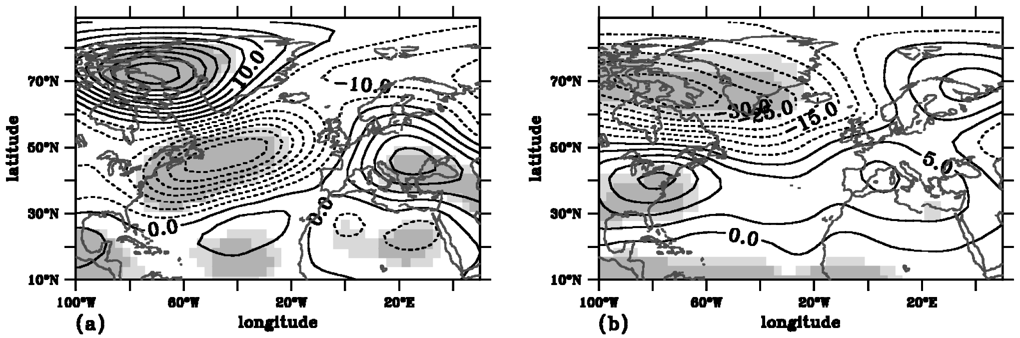

Figure 9. October and November 500 hPa geopotential-height response in (a) $P_{ML} - C_{ML}$ and (b) $N_{ML} - C_{ML}$ (see text). Contour interval 5 m. Statistical significance shading as in Fig. 4.

Nonlinear planetary-scale wave–wave interactions as defined by Kao and Lee (1977) may explain the amplitude differences of the propagating variance maxima in P_{ML} and N_{ML} with respect to C_{ML}. The interaction of propagating planetary-scale waves with the stationary waves or with the basic flow can reduce or enhance the westward-propagating-wave variance. In particular, it has been observed that when the basic flow is more zonal the variance of the westward-propagating planetary-scale waves is reduced (Doblas-Reyes, personal communication). It can thus be inferred from Fig. 8 that in the case of a zonally asymmetric large-scale response as in Fig. 5(b), the variance of the westward-propagating planetary-scale wave of the model can be enhanced. Those findings confirm the wave-like nature of the response and the nonlinear interactions of the wave-like response with the stationary waves or the mean flow. Those interactions are associated with an asymmetrical response in wave variance, with respect to the sign of the forcing.

We can conclude at this stage that the mean ON linear response is significant in both types of experiments and amplified in L_{ML}. The model response reproduces well the observed linear relationship between the equatorial SST mode and the NAO, although it does not persist significantly until NDJ. The wave response is stronger and more significant in L_{ML}, which suggests that a positive feedback is taking place in L_{ML} with respect to L. This feedback could be due to the thermal coupling with the slab ocean in the midlatitudes, which is the only difference between the experiments. This coupling could reinforce the middle- and high-latitude atmospheric-circulation anomalies initiated by the wave response to the tropical SST anomaly. To investigate this possible feedback, as well as the asymmetry of the wave-variance response, we now focus on the midlatitude response to positive or negative autumn tropical SST anomalies in P_{ML} and N_{ML}, respectively, with respect to the C_{ML} control experiment. The ON P_{ML} and N_{ML} Z500 responses (respectively, Figs. 9(a) and (b)) are both statistically significant at large scales. Their spatial structures are quite symmetrical with respect to the sign of the SST forcing in the western part of the North Atlantic, and over the Labrador Sea. In contrast, both responses have the same sign over Europe and the Mediterranean Sea, and the N_{ML} response is not statistically significant in this region. The P_{ML} Z500 response spatial structure is a north-westward-arching wave, originating in the central tropical Atlantic, over the prescribed warm SST anomaly. The N_{ML} Z500 response is closer to the observed (Fig. 2(a)) and modelled (Fig. 2(c)) NAO pattern in this season, than the P_{ML} response. As can be seen in Fig. 10, the surface heat-flux exchanges between the atmospheric response to the equatorial SST

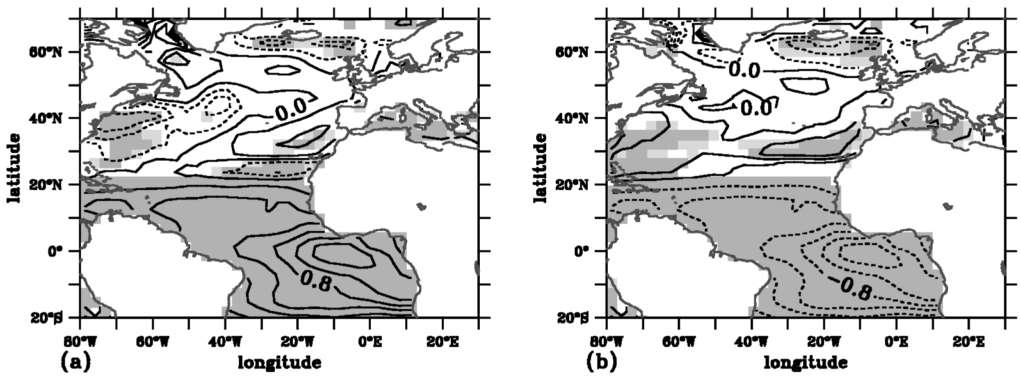

Figure 10. October and November surface-temperature response in (a) $P_{ML} - C_{ML}$ and (b) $N_{ML} - C_{ML}$ (see text). Contour interval 0.2 degC. Statistical significance shading as in Fig. 4.

anomaly, and the midlatitude mixed layer induce SST anomalies in the extratropics in ON. These anomalies are symmetrical with respect to the tropical SST forcing only in the western part of the basin between 20 and 40°N. In P_{ML}, the 40°N low induces a negative latent-heat flux anomaly (not shown) meaning that the ocean loses heat, and thus a cold SST anomaly. In N_{ML} a positive downward latent-heat flux anomaly warms up the mixed layer over a latitudinal band (20°N to 40°N). In the next section, we examine the asymmetrical response in the midlatitudes in detail, and especially assess if it can be interpreted in terms of weather-regime changes. We then examine local atmospheric physical processes, such as transient-eddy processes, that can interact with the mean flow and modulate the response, and see if they could play a role in this asymmetry.

(*b*) *Asymmetrical modulation of the response in the midlatitudes*

(i) *An asymmetrical high-frequency response.* As the midlatitude part of the response is equivalent barotropic, we choose to study the high-frequency and asymmetrical response at the surface, doing a weather-regime analysis on the SLP. The frequency of occurrence of the intrinsic NAE sector daily SLP weather regimes of the model are thus estimated in the different ensembles with a cluster classification of the SLP daily maps, as explained in section 2(d). The composite SLP maps of the weather regimes obtained in every case are displayed in Fig. 11. Sea-level-pressure maps of the various experiments are thus classified into positive and negative phases of the NAO, and of the east Atlantic mode (respectively north/east Atlantic ridge and low).

The percentages of occurrence of the four regimes of Fig. 11 are displayed in Fig. 12(a) for P, N, and C classified together. The only significant response is the reduction of the frequency of occurrence of the negative NAO regime in N, which is larger than the error margin of about 5%. The mean linear part of the Z500 response to the N forcing can be estimated by the opposite of the Fig. 5(a) pattern, and thus should be close to a positive phase of the NAO. Although weak, the NAO regime-occurrence changes in response to the N SST forcing (less negative and more positive phases) are thus consistent with the mean linear response. Changes in the north/east Atlantic ridge (EA ridge) occurrences are negligible, whereas there is a strong enhancement of the percentage of occupation of the north/east Atlantic Low (EA low) regime in P, and more

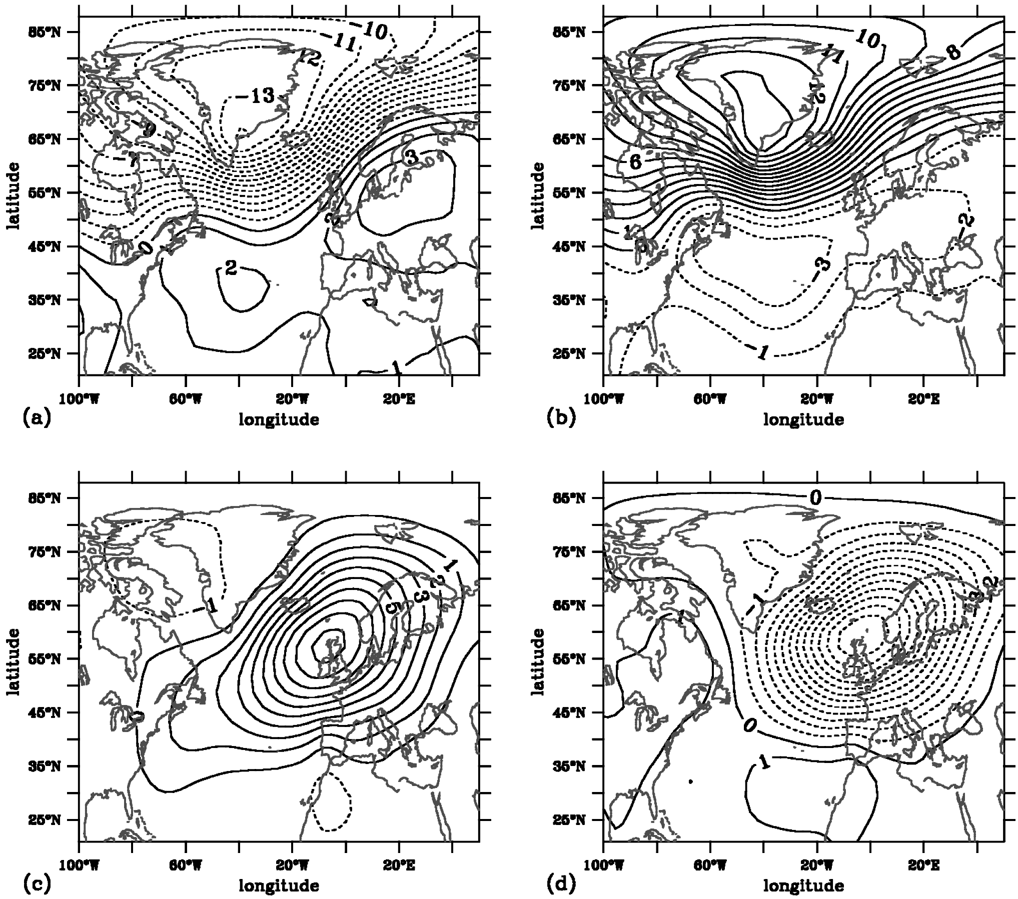

Figure 11. October and November sea-level-pressure daily map composites of the daily weather regimes k-means classifications of the various experiments (here P_{ML}, N_{ML} and C_{ML} classified together, see text). Contour interval 1 hPa. (a) Positive North Atlantic Oscillation (NAO) regime, (b) negative NAO regime, and north/east Atlantic (EA) (c) ridge and (d) low regimes.

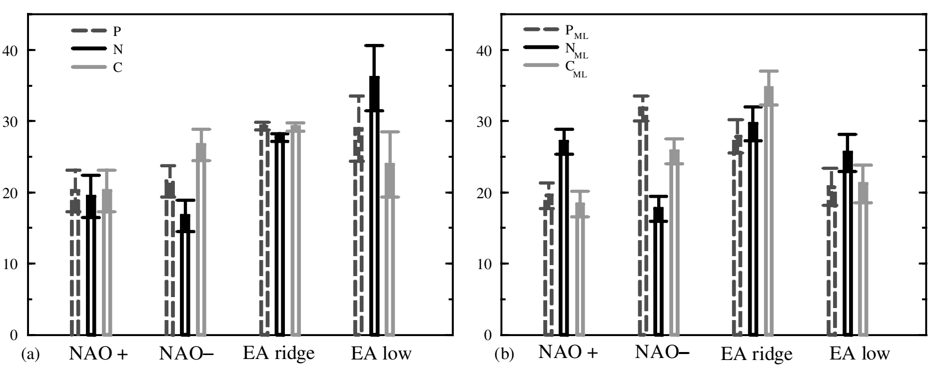

Figure 12. Percentages of daily occurrences in October and November of the different regimes displayed in Fig. 11, (a) in the P, N and C experiments classified together, and (b) in the P_{ML}, N_{ML} and C_{ML} ensembles classified together (see text). The classification method and computation of the error bars are described in section 2(d).

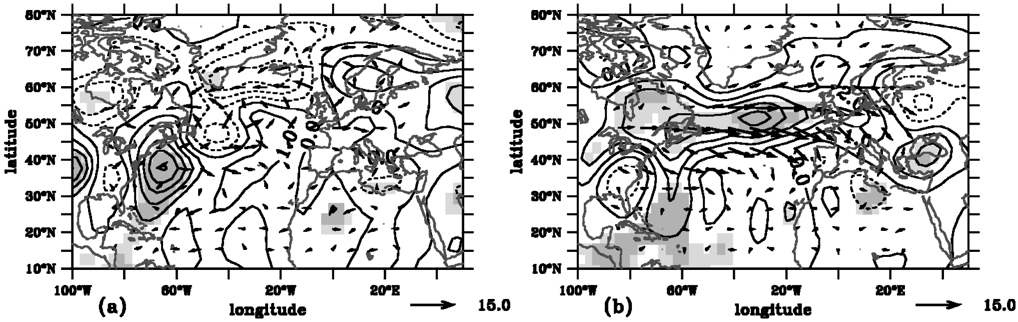

Figure 13. October and November Storm-Track Activity (STA) $\sqrt{\overline{z'^2}}$ response (contour interval 1 m) and regressed Eliassen–Palm vector **E** response (m^2s^{-2}) in (a) $P_{ML} - C_{ML}$ and (b) $N_{ML} - C_{ML}$ (see text). Statistical significance shading as in Fig. 4.

significantly in N with respect to C. The latter is difficult to interpret as the EA low and the negative NAO phase are both spatially correlated with the linear response.

The P_{ML} and N_{ML} responses in terms of change of frequency of occurrence of the NAO phases (Fig. 12(b)) are clearer than the P- and N-forced ensemble's responses. The changes of percentages of occurrence of the NAO regimes in N_{ML} are nearly twice the error margin of about 5%. Consistent with the linear response of Fig. 5(b), the positive NAO regime occurrence increases as that of the negative decreases in N_{ML}. In P_{ML}, the NAO regime occurrences are not significantly different from the C_{ML} ones. The occurrence of the EA ridge and low regimes is not significantly changed in either P_{ML} or N_{ML} with respect to C_{ML}.

We have seen in Fig. 9 that the spatial structure of the N_{ML} mean Z500 response with respect to the control simulation C_{ML} was closer to the NAO pattern than the P_{ML} response. The N_{ML} mean response can thus be interpreted as resulting from an asymmetrical high-frequency response in terms of the change in the frequency of occurrence of the NAO weather regimes. The P_{ML} forcing was shown to induce more propagating-wave activity than N_{ML}, consistent with the arching wave structure of the P_{ML} Z500 response (Fig. 9(a)). This propagating nature could explain why the P_{ML} mean response can not be interpreted clearly by a change in the frequencies of occurrence of the regimes. Another important point is that the mean response together with the weather-regime interpretation is much clearer in the case of a thermal coupling in the midlatitudes. In the case of a negative SST forcing in the tropics, a positive SST anomaly appears in the mixed layer at 40°N. This SST anomaly is likely to reinforce the SST gradient off Newfoundland, and the hypothesis can be made that it interacts with the atmospheric mean circulation and transients, and strengthens the positive phase of the NAO.

(ii) *An asymmetrical response in transient-eddy activity in the coupled ensembles.* In section 3(a), a frequency–wave-number spectral analysis on the sensitivity experiments' Z500 fields points out the planetary-scale wave's activity induced by the equatorial SST forcing in ARPEGE. Differences in propagating-wave variances of smaller amplitude are also captured at higher frequencies in the synoptic domain (periods from 3 to 5 days, $k = 2$–4). The comparison between synoptic propagating variance of the forced and coupled sensitivity experiments shows that the synoptic wave's variance is enhanced in both N_{ML} and P_{ML}, while in P and N there is no significant change with respect to the control C (not shown).

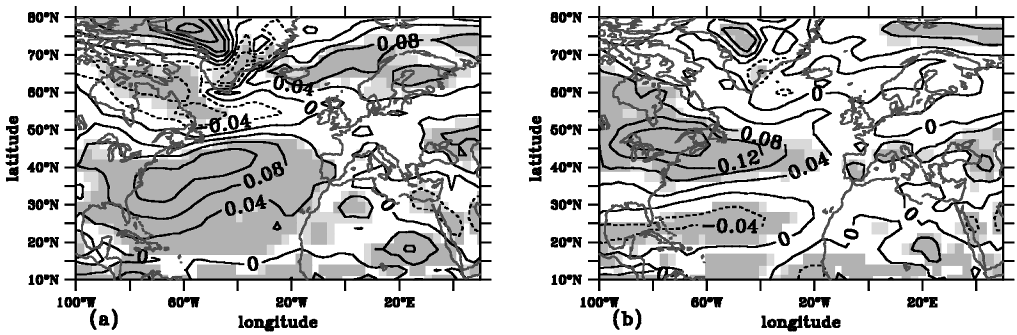

Figure 14. October and November Eady growth rate of baroclinic instabilities σ_{BI} response in (a) $P_{ML} - C_{ML}$ and (b) $N_{ML} - C_{ML}$ (see text). Contour interval 0.04 day^{-1}. Statistical significance shading as in Fig. 4.

The spatial structure of the associated perturbation of the synoptic activity can be observed in the STA L_{ML} response (not shown), and more clearly in P_{ML} and N_{ML} anomalies of STA with respect to C_{ML} displayed in Fig. 13. In P_{ML} the maximum of STA is located between 25°N and 45°N east of the North American coasts, with a secondary maximum downstream to the north-east, near 50°N. Conversely, in N_{ML} the 50°N STA is enhanced and there is a reduction of activity on the 20°N–45°N latitude band. This northward shift is consistent with the signature of a positive phase of the NAO, the synoptic weather system's movement being connected with the westerly mean flow. These anomalous transient eddies are thus likely to reinforce the low-frequency anomalous circulation induced in P_{ML} and N_{ML} by the Z500 responses of Fig. 9. The low-frequency geostrophic circulation is reinforced in P_{ML} near 40°N and north-eastward downstream, by means of convergence of transient-eddy momentum, as diagnosed by the divergence of the regressed **E** vector in Fig. 13(a) (see section 2 for the interpretation of the **E** vectors). In N_{ML}, the divergence of the **E** vectors is clearer and stronger, and is localized off Newfoundland and downstream near 50°N, as can be seen in Fig. 13(b).

This transient-eddy anomalous activity is linked with changes in baroclinicity, as can be seen in the Eady growth rate of baroclinic instabilities σ_{BI} P_{ML} and N_{ML} anomalies (Fig. 14). The spatial asymmetries of the σ_{BI} responses are consistent with the STA response. A local increase of σ_{BI} takes place for both signs of the forcing in the western part of the basin, with more eastward extension of the anomalies in Fig. 14(a) for the P_{ML} forcing. In this ensemble, the baroclinicity is enhanced in the western part of the basin between 25°N and 50°N and reduced over the 50°N to 60°N latitude band, suggesting a slight southward shift of the baroclinicity maximum. In N_{ML}, a northward shift can be seen, with a reduction of baroclinicity between 20°N and 30°N, and a positive anomaly between 35°N and 55°N. Those changes in baroclinicity are linked to the different SST anomalies that are generated in the oceanic mixed layer in Fig. 6, but are also associated with spatial asymmetries in the wind-shear changes (not shown). Consistent with Peng *et al.* (1995), we suggest that the asymmetry in the midlatitude response may be in part explained by the climate-mean state characteristics of ON, where the strong climatological SST gradient near 50°N induces a local baroclinicity maximum, together with the North Atlantic 'eddy driven' jet stream. The latter is shifted slightly north of its later winter position and thus increases the zonal wind shear near 50°N. A second wind-shear maximum is situated near 15°N, associated with the subtropical jet stream. In the P_{ML} ensemble, the 200 hPa zonal wind is enhanced between 20°N and 40°N (not shown), consistent with Fig. 13(a), and with the L_{ML} 200 hPa zonal-wind linear response of Fig. 7. In N_{ML}, the zonal-wind response is a positive anomaly in the North Atlantic over a latitude band near 50°N and a negative one at 20°N (not shown), consistent with Fig. 13(b) and an enhancement of the 'eddy driven' jet stream. As can be seen in Fig. 10, the SST gradient is reinforced in P_{ML} near 25°N, whereas in N_{ML} it is near 50°N. These diagnostics all together show that a strong interaction takes place near 50°N in N_{ML} between the transient eddies, the eddy-driven jet and the mid- and high-latitude part of the wave response, and the oceanic mixed layer. This interaction is concomitant with the asymmetry of the high-frequency midlatitude response. In P_{ML}, an interaction between the subtropical jet, the transient eddies and the SST gradient is also diagnosed, but is not associated with a strengthening of the mid–high-latitude atmospheric circulation.

Consistent with the results of Peng and Whitaker (1999), these results suggest that the transient eddies can be a major factor in the modulation of the response depending on the background state. Walter *et al.* (2001) also show that shifting the position of the cold (warm) SST anomaly poleward or equatorward with respect to an idealized storm track induces an enhancement (reduction) of the response. This kind of spatial asymmetry might also have an influence here.

4. Mean January and February modelled response to the midlatitude SST

In order to confirm the Czaja and Frankignoul (2002) hypothesis, we now focus on the winter JF delayed response to the autumn tropical SST anomaly. As the JF atmospheric and mixed-layer (in the coupled case) responses are only significant in the case of a negative anomaly in the tropics, we do not show the P_{ML} and P insignificant responses and restrict our following comments to the N_{ML} and N responses.

The N_{ML} midlatitude SST anomaly that can be seen in ON (Fig. 10(b)) persists until JF (Fig. 15(a)) with its maximum shifted south from 30°N to 25°N. As first seen in Fig. 4(b), the JF L_{ML} Z500 linear response is not statistically significant. However, the N_{ML} atmospheric response with respect to C_{ML} (Fig. 15(b)) is a significant latitudinal dipole close to a positive phase of the observed NAO, with a very strong and significant cyclonic anomaly centred south of Greenland at 40°W and 60°N, slightly south of that observed. However, this structure is more zonal and shifted to the south compared with the model NAO as defined for JF by the first EOF of C_{ML} (Fig. 2(e)). The mean JF Z500 response in the forced ensembles P and N with respect to the control simulation C, can be interpreted as the model's instantaneous response to either sign of the winter SST tripole. The Z500 response to the tripole with a positive central anomaly (N ensemble) is significant in JF and has comparable amplitude and features to the N_{ML} ensemble, but with more penetration into the European continent. This asymmetry in both coupled and forced ensembles explains why we do not see any significant response in L or L_{ML} in JF in Fig. 4. Although neither an N_{ML} nor a P_{ML} significant response in STA can be seen in JF (not shown), the 200 hPa wind response in the N_{ML} ensemble in Fig. 15(b) is consistent with a strengthening of the eddy-driven jet stream. In contrast, we have seen that there is a significant STA response in ON in the coupled model, especially in the case of a negative anomaly in the tropics (Figs. 13 and 14). The hypothesis can thus be maintained that in N_{ML}, an anomalous interaction between the transient eddies and the mean flow takes place in ON, that can play a role in the persistence of the SST anomaly in the mixed layer. Both the SST anomaly in the mixed layer and the anomalous atmospheric circulation are persistent only when associated with a significant anomalous transient-eddy-activity response. These results all together suggest that the interaction

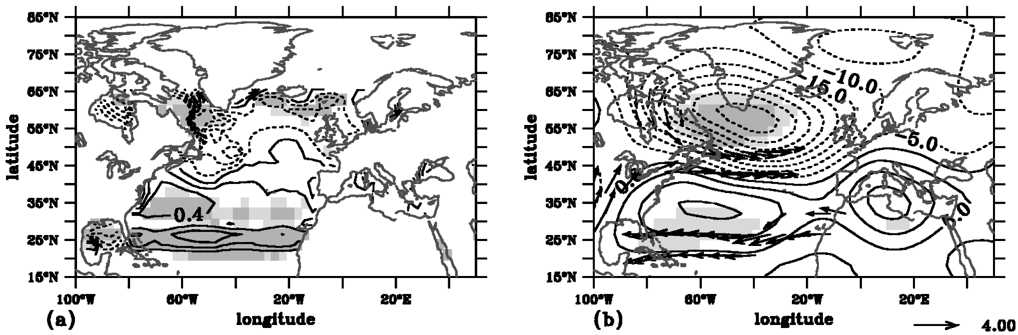

Figure 15. $N_{ML} - C_{ML}$ (see text) January and February (a) sea surface temperature (SST) response (contour interval 0.2 degC), and (b) 500 hPa geopotential-height response (contour interval 5 m, shading as in Fig. 4) with superimposed 200 hPa wind response (m s^{-1}) if significant at more than 90%.

between the three is important in reproducing the observed response. We also obtain a structure resembling the observed response to the tropical anomaly by forcing with the tripole SST anomaly in winter, and only in the N case, which suggests that the JF atmosphere is sensitive to this type of forcing. Terray and Cassou (2002) suggest that the subtropical part of the tripole can play an important role in this sensitivity.

5. Conclusions

The midlatitude atmospheric and oceanic mixed-layer responses to an observed autumn tropical Atlantic SST anomaly are studied with a set of model experiments. A Rossby wave arching from central America and the Caribbean Sea to the NAE region is observed in the ARPEGE AGCM mean autumn (ON) synchronous response to the SST anomaly. The tropical Atlantic positive SST forcing initiates an anomalous convergence of heat and humidity in the Amazon region that reinforces convection and thus induces divergence at altitude. This anomalous divergence alters the local Hadley circulation and anomalous vorticity is advected to the north. Associated perturbations of the jet stream near the subsiding branch of the Hadley cell then induce a Rossby wave ending in a cyclonic anomaly over the North Atlantic basin. Comparison between sensitivity experiments, with and without coupling of ARPEGE with a North Atlantic oceanic mixed layer suggests that the air–sea coupling plays an important role in the maintenance and amplification of the response at the middle and high latitudes. Thermal coupling allows the atmospheric wave-like response to the tropical SST forcing to imprint SST anomalies in the North Atlantic. In the case of a negative SST anomaly in the tropics, the wind-shear anomalies associated with the wave response, together with the SST anomaly induced in the mixed layer, are likely to induce more baroclinicity in a region that is critical for the development of synoptic perturbations. The negative anomaly in the tropics thus triggers an interaction between the oceanic mixed layer, the storm-track activity and the mean wave-like response which is close to the positive phase of the NAO in the midlatitudes. Moreover, a weather-regime analysis shows that the mean autumn response in this case can be interpreted in terms of changes in the frequency of occurrence of the model's intrinsic regimes, as the positive (negative) NAO phase occurs far more (less) often. An important result of this study is that in the case of a negative tropical SST anomaly the SST and Z500 responses persist until winter (JF). The midlatitude part of the atmospheric winter response then resembles the positive phase of the NAO at this season. Despite its nonlinear nature, this lagged response is consistent with the linear statistical link found by Czaja and Frankignoul (2002) between the autumn SST anomaly and the winter NAO.

The asymmetry of the response is connected with the seasonal characteristics of the atmospheric background flow and thus, considering the model biases, might be model dependent. Although the number of members is suitable for studies of SST sensitivity to tropical SST anomalies, it might not be enough to extract the midlatitude atmospheric response in the case of an atmosphere–ocean thermal coupling in the midlatitudes. An intercomparison between different model sensitivity studies to these anomalies is thus needed for a confirmation of these results, as well as to better understand the processes. In particular, the link between the SST anomaly and the jet-stream perturbations could be investigated. They might be linked together by a local Hadley cell perturbation as proposed here, but as suggested by Held *et al.* (1989) anomalous upper-level subtropical transients in response to the tropical SST anomaly might also induce the subtropical jet-stream fluctuations.

ACKNOWLEDGEMENTS

The authors are grateful to the anonymous reviewers for their considerable help in improving the manuscript. They wish to thank F. J. Doblas-Reyes for helpful discussions, and for the space–time spectral-analysis program. They are also grateful to Michel Déqué for providing the ARPEGE model, and to Jean Philippe Piedelièvre and Fabien Crépin for carrying out the coupling of ARPEGE with a slab ocean. This work was supported by the EC-PREDICATE project under contract EVK2-CT-1999-00020.

REFERENCES

Bjerknes, J. 1964 Atlantic air–sea interaction. *Adv. in Geophys.*, **10,** 1–82

Cassou, C. and Terray, L. 2001 Oceanic forcing of the wintertime low frequency atmospheric variability in the North Atlantic European sector: A study with the ARPEGE model. *J. Climate*, **14,** 4266–4291

Cayan, D. R. 1992 Latent and sensible heat flux anomalies over the northern oceans: Driving the sea surface temperature. *J. Phys. Oceanogr.*, **22,** 859–881

Corti, S., Molteni, F. and Palmer, T. N. 1999 Signature of recent climate change in frequencies of natural circulation regimes. *Nature*, **398,** 799–802

Czaja, A. and Frankignoul, C. 1999 Influence of the North Atlantic SST on the atmospheric circulation. *Geophys. Res. Lett.*, **26,** 2969–2972

2002 Observed impact of Atlantic SST anomalies on the North Atlantic Oscillation. *J. Climate*, **15,** 606–623

Déqué, M., Dreveton, C., Braun, A. and Cariolle, D. 1994 The ARPEGE/IFS climate model: A contribution to the French community climate modelling. *Clim. Dyn.*, **10,** 249–266

Doblas-Reyes, F. J., Déqué, M., Valero, F. and Stephenson, D. B. 1998 North-Atlantic wintertime intraseasonal variability and its sensitivity to GCM horizontal resolution. *Tellus*, **50A,** 573–595

Doblas-Reyes, F. J., Pastor, M. A., Casado, M. J. and Déqué, M. 2001 Wintertime westward-traveling planetary scale perturbations over the Euro-Atlantic region. *Clim. Dyn.*, **17,** 811–824

Drévillon, M., Terray, L., Rogel, P. and Cassou, C. 2001 Midlatitude Atlantic SST influence on European winter climate variability in the NCEP reanalysis. *Clim. Dyn.*, **18,** 331–344

Farrara, J. D., Mechoso, C. R. and Robertson, A. W. 2000 Ensembles of AGCM two-tier predictions and simulations of the circulation anomalies during winter 1997–98. *Mon. Weather Rev.*, **128,** 3589–3604

Fraedrich, K., Bantzer, C. and Burkhardt, U. 1993 Winter climate anomalies in Europe and their associated circulation at 500 hPa. *Clim. Dyn.*, **8,** 161–175

Frankignoul, C. 1985 Sea surface temperature anomalies, planetary waves, and air–sea feedback in the middle latitudes. *Rev. Geophys.*, **23,** 357–390

Hayachi, Y. 1971 A generalized method of resolving disturbances into progressive and retrogressive waves by space Fourier and time cross-spectral analyses. *J. Meteorol. Soc. Jpn*, **49,** 125–128

Hoerling, M. P. and Ting, M. 1994 Organization of extratropical transients during El Niño. *J. Climate*, **7,** 745–766

Held, I. M., Lyons, S. W. and Nigam, S. 1989 Transients and the extratropical response to El Niño. *J. Atmos. Sci.*, **46,** 163–174

Hoskins, B. J. and Ambrizzi, T. 1993 Rossby wave propagation on a realistic longitudinally varying flow. *J. Atmos. Sci.*, **50,** 1661–1671

Hoskins, B. J. and Valdes, P. J. 1990 On the existence of storm-tracks. *J. Atmos. Sci.*, **47,** 1854–1864

Hurrell, J. W., Hack, J. J., Boville, B. A., Williamson, D. L. and Kiehl, J. T. 1998 The dynamical simulation of the NCAR Community Climate Model Version 3 (CCM3). *J. Climate*, **11,** 1207–1236

Kao, S. K. and Lee, H. N. 1977 The nonlinear interactions and maintenance of the large-scale moving waves in the atmosphere. *J. Atmos. Sci.*, **34,** 471–485

Lau, N.-C. 1997 Interactions between global SST anomalies and the midlatitude atmospheric circulation. *Bull. Am. Meteorol. Soc.*, **78,** 21–33

Michelangeli, P. A., Vautard, R. and Legras, B. 1995 Weather regime recurrence and quasi stationarity. *J. Atmos. Sci.*, **52,** 1237–1256

Peng, S. and Robinson, W. A. 2001 Relationships between atmospheric internal variability and the responses to an extratropical SST anomaly. *J. Climate*, **14,** 2943–2959

Peng, S. and Whitaker, J. S. 1999 Mechanisms determining the atmospheric response to midlatitude SST anomalies. *J. Climate*, **12,** 1393–1408

Peng, S., Mysak, L. A., Ritchie, H., Derome, J. and Bugas, B. 1995 The differences between early and midwinter atmospheric responses to sea surface temperature anomalies in the northwest Atlantic. *J. Climate*, **8,** 137–157

Plumb, R. A. 1985 On the three-dimensional propagation of stationary waves. *J. Atmos. Sci.*, **42,** 217–228

Pratt, R. W. 1976 The interpretation of space time spectral quantities. *J. Atmos. Sci.*, **33,** 1060–1066

Qin, J. and Robinson, W. A. 1993 On the Rossby wave source and the steady linear response to tropical forcing. *J. Atmos. Sci.*, **50,** 1819–1823

Rodwell, M. J. and Folland, C. K. 2002 Atlantic air–sea interaction and seasonal predictability. *Q. J. R. Meteorol. Soc.*, **128,** 1413–1443

Sardeshmukh, P. D. and Hoskins, B. J. 1988 The generation of global rotational flow by steady idealized tropical divergence. *J. Atmos. Sci.*, **45,** 1228–1251

Sutton, R. T., Jewson, S. P. and Rowell, D. P. 2000 The elements of climate variability in the tropical Atlantic region. *J. Climate*, **13,** 3261–3284

Terray, L. and Cassou, C. 2002 Tropical Atlantic sea surface temperature forcing of the quasi-decadal variability over the North Atlantic European region. *J. Climate*, **22,** 3170–3187

Trenberth, K. E. 1986 An assessment of the impact of transient eddies on the zonal flow during a blocking episode using localized Eliassen–Palm flux diagnostics. *J. Atmos. Sci.*, **43,** 2070–2087

Trenberth, K. E., Branstator, G. W., Karoly, D., Kumar, A., Lau, N.-C. and Ropelewski, C. 1998 Progress during TOGA in understanding and modeling global teleconnections associated with tropical sea surface temperatures. *J. Geophys. Res.*, **103,** 14291–14324

Tyrrell, C. G., Karoly, D. J. and McBride, J. L. 1996 Links between tropical convection and variations of the extra-tropical circulation during TOGA-COARE. *J. Atmos. Sci.*, **53,** 2735–2748

Von Storch, H. and Zwiers, F. W. 1999 *Statistical analysis in climate research*. Cambridge university press, Cambridge

Walter, K., Luksch, U. and Fraedrich, K. 2001 A response climatology of idealized midlatitude thermal forcing experiments with and without a storm track. *J. Climate*, **14,** 467–484

Watanabe, M. and Kimoto, M. 1999 Tropical–extratropical connection in the Atlantic atmosphere–ocean variability. *Geophys. Res. Lett.*, **26,** 2247–2250

Zebiak, S. E. 1993 Air–sea interaction in the equatorial Atlantic region. *J. Climate*, **6,** 1567–1586